FDTD ANALYSIS OF A CONICAL MICROSTRIP ANTENNA ON EBG SUBSTRATE

G. S. Kliros, G. Kyritsis and D. Touzloudis

Hellenic Air-Force Academy, Department of Aeronautical Sciences
Division of Electronics and Communication Engineering
Dekeleia Air-Force Base, Attica GR-1010, Greece
gsksma@hol.gr

Abstract

In this paper, the finite difference time domain method in spherical coordinates is used to analyze a microstrip conical antenna with a dielectric electromagnetic band-gap (EBG) structure as substrate. The voltage standing wave ratio, matched impedance, maximum gain as well as far-field radiation patterns, are presented. Our study suggests that the microstrip conical antenna on EBG substrate holds sufficient potential as a low-profile antenna with very wideband and high gain characteristics. A time domain study has shown that the antenna distorts the excitation pulse in a moderate way. These features make the proposed antenna suitable for both ultra-wide band systems and as wind-band scan antenna.

1. INTRODUCTION

The need of ultra-wideband (UWB) antennas is increasing for both military and commercial applications [1]. The UWB radio technology promises high resolution radar applications, sensor networks with a large number of sensors as well as high data rate communication over short range for personal area networks. With a need for antennas with the characteristics of broad bandwidth and small electrical size, conical antenna structures have been a focus of research [2,3]. Moreover, microstrip conical antennas are of significant importance due to conformal capability attributed to their low profile structure [4].

Microstrip conical antennas on uniform dielectric substrates have been proposed and analysed [5]. Dielectric or magnetic conical substrate enables making the antenna electrically smaller and more rugged but cannot improve the radiation efficiency and gain of the antenna. Electromagnetic band-gap (EBG) structures are periodic metallic or dielectric materials that can control the propagation of electromagnetic waves whatever the direction of propagation is. They gained a growing interest in the antenna domain since they have been used as substrates or superstrates in order to improve planar antenna performances [6,7]. Recently, EBG structures have been used as ground planes to produce a uni-directional beam from wideband dipoles with good gain [8].

In this study, a mirpostrip conical antenna on a dielectric EBG substrate and placed above a ground plane, is investigated numerically. A FDTD in-house code in spherical coordinates is developed to simulate this novel conical microstrip antenna. Results concerning VSWR, input impedance, maximum gain and far-field radiation patterns are presented. For evaluating waveform distortions, a time-domain study is also presented.

2. ANTENNA DESIGN AND SIMULATION METHOD

The geometry of the proposed conical microstrip antenna on EBG substrate is illustrated in Fig. 1 and is described by the following parameters: the semi-cone angle (flare angle) θ_0, the free-space semi-cone angle θ_{free}, the length of the antenna's arm ℓ_{ant} and the substrate length ℓ_{sub}. The EBG sub-strate is made of cylindrical shells with alternating high (Rogers-TMM4:ε_r = 9.8) and low (RT-Duroid, ε_r= 2.2) permittivity materials with their thickness equal to $\lambda_g/4$ (designed at the central frequency of operating band). The antenna is fed at the tip of the cone by a coaxial cable. It is a rotationally symmetric and is excited by rotationally symmetric source. In order to analyse and optimize the antenna for UWB radio technology, a FDTD code in spherical coordinates is implemented in Matlab following the lines of Ref. [9].

Since the antenna has rotational symmetry about the *z*-axis, there are no azimuth angle dependencies and therefore, there are three field components: E_r, E_θ and H_ϕ. Using the FDTD me-

thod on a modified Yee cell [9], a set of discrete field equations is obtained:

$$E_r^{n+1}(i,j)=C_a(i)E_r^n(i,j)+\frac{C_b(i)}{(i+1/2)\Delta\theta} \times\left[\frac{\sin((j+1/2)\,\Delta\theta)}{\sin((j-1/2)\,\Delta\theta)}H_\phi^{n+\frac{1}{2}}(i,j)-H_\phi^{n+\frac{1}{2}}(i,j-1)\right] \quad (1)$$

$$E_\theta^{n+1}(i,j)=C_a(i)E_\theta^n(i,j)+ +C_b(i)\cdot\left[H_\phi^{n+\frac{1}{2}}(i-1,j)-\left(\frac{i+1/2}{i-1/2}\right)\cdot H_\phi^{n+\frac{1}{2}}(i,j)\right] \quad (2)$$

$$H_\phi^{n+\frac{1}{2}}(i,j)=D_a(i)H_\phi^{n-\frac{1}{2}}(i,j)+\frac{D_b(i)}{(i+1/2)\Delta\theta} \times\left[\frac{\sin((j+1)\Delta\theta)}{\sin(j\,\Delta\theta)}E_r^n(i,j+1)-E_r^n(i,j)\right] -D_b(i)\left[\left(\frac{i+1}{i}\right)E_\theta^n(i+1,j)-E_\theta^n(i,j)\right] \quad (3)$$

where,

$$C_a(i)=\frac{1-\frac{\sigma_i\,\Delta t}{2\varepsilon_i}}{1+\frac{\sigma_i\,\Delta t}{2\varepsilon_i}},\quad C_b(i)=\frac{\frac{\Delta t}{\varepsilon_i\,\Delta r}}{1+\frac{\sigma_i\,\Delta t}{2\varepsilon_i}}, \quad (4)$$

$$D_a(i)=\frac{1-\frac{\sigma_i^*\Delta t}{2\mu_i}}{1+\frac{\sigma_i^*\Delta t}{2\mu_i}},\quad D_b(i)=\frac{\frac{\Delta t}{\mu_i\,\Delta r}}{1+\frac{\sigma^*\Delta t}{2\mu_i}} \quad (5)$$

and, Δr and $\Delta\theta$ represent the step size in the r- and θ-directions, respectively. Superscript n signifies that the quantities are to be evaluated at $t = n\Delta t$, and, i and j represent the point ($i\Delta r$, $j\Delta\theta$) in the spherical grid. The half-time steps indicate that the fields are calculated alternately. The maximum time step is limited by the stability Courant's criterion:

$$\Delta t\le\min\frac{r\,(\Delta r)(\Delta\theta)}{c_0\sqrt{(\Delta r)^2+(r\Delta\theta)^2}} \quad (6)$$

where c_0 is the velocity of the light in free space.

The base of the antenna is driven by a voltage signal $V_s(t)$ with internal resistance R_s through a coaxial line with inner and outer conductor's diameters a and b respectively. The electric driving field E_θ, resulting from the input voltage, can be written in FDTD form as

$$E_\theta^n(i,j)=-\frac{V_s(n\,\Delta t)-R_s\,I_{in}^{n-1/2}(i,j)}{b\sin(j\Delta\theta)\ln(b/a)} \quad (7)$$

where the current through the source is given by

$$I_{in}^{n-1/2}(i,j)=2\pi(i\,\Delta r)\sin\left((j+1/2)\Delta\theta\right) \times H_\phi^{n-1/2}\left(i+1/2,j+1/2\right) \quad (8)$$

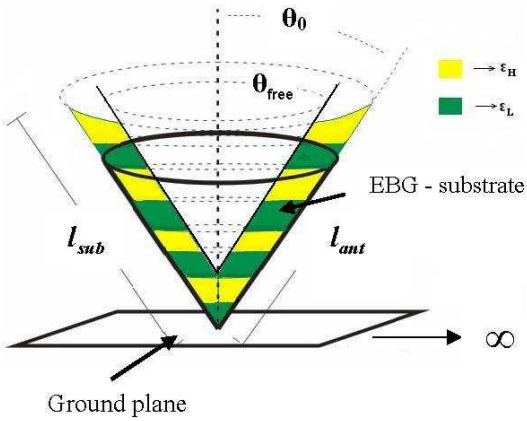

Fig. 1. Geometry of the proposed antenna

Finally, Berenger's perfectrly matched layer (PML) is applied as absorbing boundary condition where a parabolic conductivity profile in the spherical PML-region is used [10]. The formulas given above, involve only the electro-magnetic fields within the spherical-FDTD simulation space; in order to calculate radiation patterns, far-fields transfer functions as well as impulse response, the provided near field data have to be transformed to far-field data according to surface equivalence theorem.

3. RESULTS AND DISCUSSION

Parametric studies concerning both impedance and radiation characteri-stics of the designed antenna, were performed using the above described spherical-coordinate FDTD method. The FDTD cell dimensions are Δr=3 mm and $\Delta\theta$=1°. The antenna sits on top of a perfectly conducting ground plane that extends 360° in all directions for a distance of $R_m=10\,\ell_{ant}$. Just before the maximum radial distance R_m is reached, the simulation space is terminated in a PML section of thickness $20\Delta r$. The maximum refle-ction coefficient at normal incidence is chosen to be $R(0)=10^{-14}$. An UWB Gaussian pulse (with FWHM = 64 ps) modulated by a continuous sine wave carrier of frequency f_c=6.85 GHz, is used in our simulations. The time step is taken Δt = 0.2 ps, sufficient to satisfy Courant's criterion.

To verify the FDTD steady-state calculations, time-domain fields are transformed to the frequency domain by a Fast Fourier transform routine. The

code was run for a wide range of antenna's parameters combinations in an effort to find the antenna with the best match to a 50 Ω SMA-connector. With the antenna's arm length chosen to be ℓ_{ant}=21 mm substrate length ℓ_{sub}=33 mm and θ_{free}=10°, we present results for the voltage standing wave ratio (VSWR), real part of impedance and maximum gain for different flare angles θ_0 of the conical antenna. The free-space angle θ_{free}=10° corresponds to $\ell_{ant}\theta_{free} \approx \lambda_g$, so that, the microstrip type of the antenna is preserved.

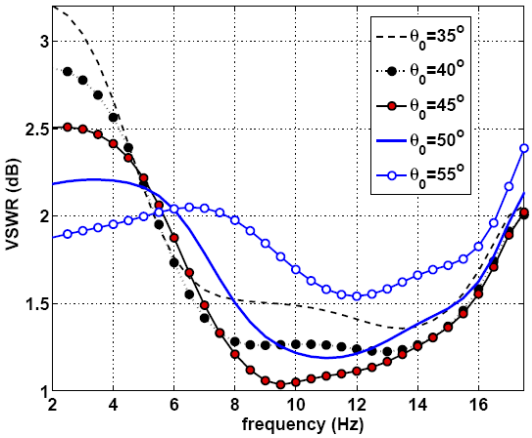

Fig. 2. Simulated VSWR for various flare angles

Fig. 3 shows the VSWR as a function of frequency where for θ_0=45° the maximum range with VSWR<1.5 is obtained. The corresponding real part of input impedance (Fig. 3) varies with the flare angle, as expected. It is observed that the optimum flare angle θ_0=45° corresponds to 50 Ω matched impedance in a frequency band from about 5.5 to 15.5 GHz.

Therefore, the designed antenna can provide more than 100% impedance bandwidth.

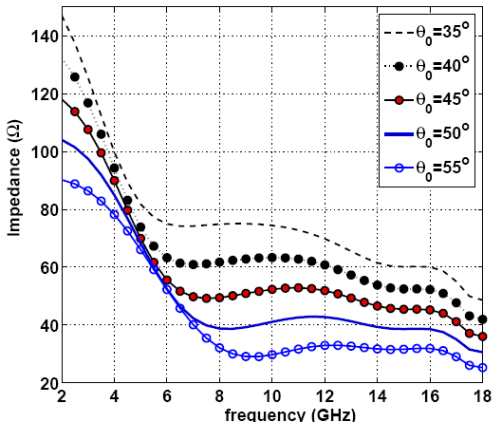

Fig. 3. Real part of input impedance for various flare angles

Fig. 4 shows the evolution of maximum gain in the elevation plane versus frequency. Gain gradually increases with frequency from 10 dBi to about 14 dBi in the frequency range from 5.5 to 7.5 GHz and ranges from 14 to 15 dBi in the frequency range from 7.5 to 15.5 GHz. Furthermore, the radiation patterns in the elevation plane (vertical polarization E_θ) are calculated in the above frequency range, although for brevity, only the patterns at 6.5, 8 and 10 GHz are shown in Fig. 5. Obviously, the radia-tion patterns are quite omni-directional but gradually degrade with increasing frequency due to the fact that the antenna's electrical size increases with frequency.

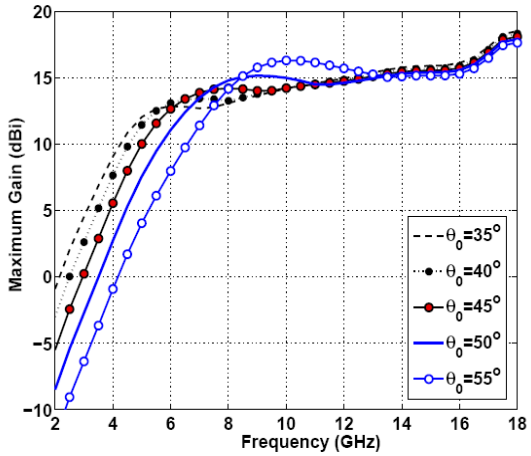

Fig. 4. Maximum gain for various flare angles

For evaluating the waveform distortions caused by the antenna, we examine the degree of similarity between source pulse and received pulse waveforms in several propaga-tion directions. Fig. 6 shows that the radiated pulse, in several radiation angular directions θ_V, is not very different from the excitation signal and therefore, antenna's fidelity in the time domain has been achieved.

The received pulse is a bit larger due to the fact that the antenna has filtered all frequencies outside the impedance bandwidth. For directions θ_V > 60°, a late-time ringing is observed that reveals a non-linearity of far-field phase. However, for a more rigorous study of pulse distortion, the linearity of far-field phase and group delay over the frequency bandwidth, should be evaluated [11,12].

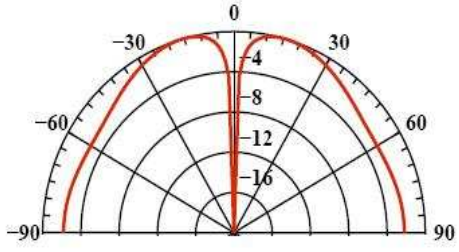

(a)

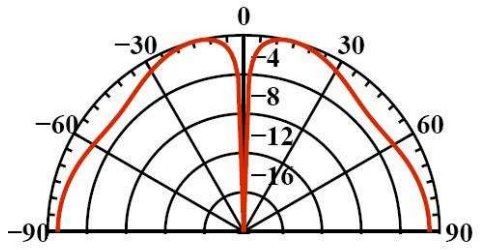

(b)

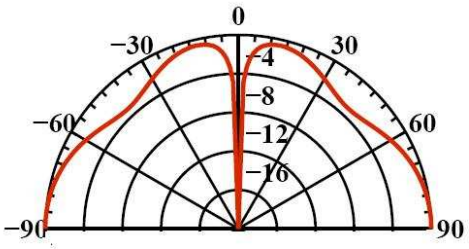

(c)

Fig. 5. Computed radiation pattern in the elevation plane at (a) f=6.5, (b) f= 8.0 and (c) f=10.0 GHz.

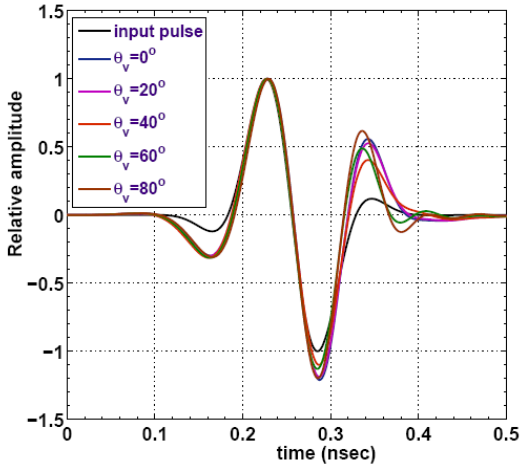

Fig. 6. Excitation and radiated pulses in different propagation directions

4. CONCLUSION

In this paper, a microstrip wideband conical antenna with a dielectric EBG substrate is proposed and analysed. A FDTD code in spherical coordinates is developed to simulate its radiation characteristics. Parametric studies lead to the optimum values of cone's arm length ℓ_{ant} =21 mm, length of substrate ℓ_{sub} =33 mm and flare angle θ_0=45^0 for 50 Ω matched impedance. This design achieves an impedance bandwidth from 5.5 to 15.5 GHz, with stable radiation patterns and a high gain of 10 to 15 dBi at the maximum radiation direction over this bandwidth. The radiation patterns are monopole-like and their frequency dependence is small in the whole UWB frequency band. A time domain study has shown that the antenna distorts the excitation pulse in a moderate way.

Consequently, our FDTD simulation suggests that a conical microstrip antenna with an EBG-substrate holds sufficient potential as a low-profile antenna with wideband and high gain characteristics.

References

[1] L. Carin and L. B. Felsen, Ultra-Wideband Short-Pulse Electromagnetics, New York, Plenum, 1995, vol.2.

[2] Y. K. Yu and J. Li, Analysis of electrically small size conical antennas, Prog. Electromag. Res. Lett., vol. 1, 2008, pp 85-92.

[3] S. Zhou, J. Ma, J. Deng, and Q. Liu, A low-profile and broadband conical antenna, Prog. in Electromag. Res. Lett., vol. 7, 2009, 97-103.

[4] Y. Lin and L. Shafai, Analysis of biconical microstrip antennas, IEE Proc.-H, vol. 139, pp. 1992, 483-490.

[5] S. Chai, D. Yao, N. Yuan, A conical microstrip antenna with uniform substrate, Int. J. Infr. Millim. Waves, Vol.18,1299-1306, 1997.

[6] G. S. Kliros, K. Liantzas, A. Konstantinidis, Modeling of Microstrip Patch Antennas with Electromagnetic Bandgap Superstrates, 19th IEEE Int. Conf. on Appl. Electrom. and Commun., Sept. 2007, Croatia, pp. 181-185.

[7] G. S. Kliros, K. Liantzas, A. Konstantinidis, Radiation Pattern Improvement of a Microstrip Patch Antenna using EBG Substrate and Superstrate, WSEAS Trans. on Commun., Vol. 6, pp. 45-52, 2007.

[8] L. Akhoondzadeh-Asl, D. Kern, P. Hall, D. Werner, Wideband Dipoles on Electromagnetic Bandgap Ground Planes, IEEE Trans. Ant. Propag. vol. 55, 2007, pp. 2426-2434.

[9] G. Liu, C. Grimes, Spherical-coordinate FDTD analysis of conical antennas mounted above finite ground planes, Microwave Opt. Techn. Lett., Vol. 23, pp 78-82, 1999.

[10] J.P. Berenger, Perfectly Matched Layer for the FDTD Solution of Wave-Structure Interaction Problems, IEEE Trans. Ant. Propag., Vol. 44, no. 1, pp 110-117, 1996.

[11] H. Ghannoum, S. Bories, C. Roblin, A. Sibille, Biconical Antennas for intrinsic characterization of the UWB channel, Proc. IEEE Int. Workshop on Antenna Technology, pp. 101-104, 2005.

[12] A. Sibille, C. Roblin, S. Bories and A. C. Lepage, A Channel-Based Statistical Approach to Antenna Performance in UWB Commun., IEEE Tran. Ant. Propag., Vol. 54, no. 11, pp. 3207-3215, 2006.